Phys Chem Minerals (2001) 28: 455–470

ORIGINAL PAPER

D. J. Frost · F. Langenhorst · P. A. van Aken

Fe–Mg partitioning between ringwoodite and magnesiowüstite and the effect of pressure, temperature and oxygen fugacity

Received: 13 September 2000 / Accepted: 25 March 2001

Abstract The partitioning of Mg and Fe between magnesiowüstite and ringwoodite solid solutions has been measured between 15 and 23 GPa and 1200–1600 °C using both Fe and Re capsule materials to vary the oxidation conditions. The partitioning results show a clear dependence on the capsule material used due to the variation in Fe^{3+} concentrations as a consequence of the different oxidation environments. Using results from experiments performed in Fe capsules, where metallic Fe was also added to the starting materials, the difference in the interaction parameters for the two solid solutions ($W^{mw}_{FeMg} - W^{ring}_{FeMg}$) is calculated to be 8.5 ± 1 kJ mol^{-1}. Similar experiments performed in Re metal capsules result in a value for $W^{mw}_{FeMg} - W^{ring}_{FeMg}$ that is apparently 4 kJ higher, if all Fe is assumed to be FeO. Electron energy-loss near-edge structure (ELNES) spectroscopic analyses, however, show Fe^{3+} concentrations to be approximately three times higher in magnesiowüstite produced in Re capsules than in Fe capsules and that Fe^{3+} partitions preferentially into magnesiowüstite, with $K^{ring/mw}_{D_{Fe^{3+}}}$ estimated between 0.1 and 0.6. Using an existing activity composition model for magnesiowüstite, a least–squares fit to the partitioning data collected in Fe capsules results in a value for the ringwoodite interaction parameter (W^{ring}_{FeMg}) of 3.5 ± 1 kJ mol^{-1}. The equivalent regular interaction parameter for magnesiowüstite (W^{mw}_{FeMg}) is 12.1 ± 1.8 kJ mol. These determinations take into account the Fe^{3+} concentrations that occur in both phases in the presence of metallic Fe. The free energy change in J mol^{-1} for the Fe exchange reaction can be described, over the range of experimental conditions, by $912 + 4.15\ (T - 298) + 18.9P$ with T in K, P in kbar. The estimated volume change for this reaction is smaller than that predicted using current compilations of equation of state data and is much closer to the volume change at ambient conditions. These results are therefore a useful test of high pressure and temperature equation of state data. Using thermodynamic data consistent with this study the reaction of ringwoodite to form magnesiowüstite and stishovite is calculated from the data collected using Fe capsules. Comparison of these results with previous studies shows that the presence of Fe^{3+} in phases produced in multianvil experiments using Re capsules can have a marked effect on apparent phase relations and determined thermodynamic properties.

Key words Ringwoodite · Magnesiowüstite · Oxygen fugacity · Element partitioning · Transition zone · High pressure

D. J. Frost (✉) · F. Langenhorst
Bayerisches Geoinstitut,
Universität Bayreuth 95440 Bayreuth, Germany
Tel.: +49-921-553737; Fax: +49-921-553769
e-mail: Dan.Frost@uni-bayreuth.de

P. A. van Aken
Institut für Mineralogie,
Technische Universität Darmstadt,
Schnittspahnstr. 9, 64287 Darmstadt, Germany

Introduction

Ringwoodite, the spinel-structured $(Mg,Fe)_2SiO_4$ polymorph, is thought to be a major constituent of the transition zone region of Earth's mantle and has also been identified in strongly shocked ordinary chondrites (Binns 1969). The breakdown of ringwoodite to produce magnesium silicate perovskite and magnesiowüstite is considered to cause the discontinuity in seismic wave velocity at 660 km which marks the top of the lower mantle. A weaker discontinuity identified at 520 km (Benz and Vidale 1993) has also been attributed to the transformation of $(Mg,Fe)_2SiO_4$ wadsleyite to ringwoodite. Due to the importance of ringwoodite in the scheme of mantle mineralogy many studies have been undertaken in order to determine its stability with respect to pressure, temperature and Fe content. Phase relations for ringwoodite have been determined by multianvil quench experiments (Ito and Takahashi 1989; Katsura and Ito 1989; Katsura et al. 1998) and the end-member reactions

have been studied using in situ techniques (Yagi et al. 1987; Irifune et al. 1998; Suzuki et al. 2000). Spectroscopic (Chopelas et al. 1994) and calorimetric measurements (Akaogi et al. 1989, 1998) of thermodynamic properties have also been used to construct internally consistent phase diagrams for ringwoodite at high pressure. Fei et al. (1991) and Matsuzaka et al. (2000) used Fe–Mg partitioning experiments to determine activity composition relations for the ringwoodite solid solution in order to refine the Mg_2SiO_4–Fe_2SiO_4 phase diagram. Studies have also considered the effects of components other than FeO and MgO on important mantle phase transformations. Wood and Rubie (1996), for example, examined the influence of Al_2O_3 on phase stability and composition either side of the 660-km discontinuity.

To date, however, very little work has focused on the possible effect of Fe^{3+} on the stability of major mantle phases such as ringwoodite and magnesiowüstite. While olivine can accommodate very little Fe^{3+}, several studies have reported that the higher-pressure polymorphs, wadsleyite and ringwoodite, can contain quite significant amounts. Canil et al. (1991) and Woodland and Angel (2000), for example, have shown that there is a complete solid solution at pressures above 9 GPa between Fe_2SiO_4 and Fe_3O_4. Using Mössbauer spectroscopy, O'Neill et al. (1993) measured significant levels of Fe^{3+} in end-member Fe_2SiO_4 ringwoodite ($Fe^{3+}/\Sigma\ Fe = 0.07$) even in the presence of metallic Fe. Magnesiowüstite can also contain significant Fe^{3+} concentrations that vary as a function of oxygen fugacity and MgO content. Measurements on wüstite in equilibrium with metallic Fe, for example, show that Fe^{3+}/Σ Fe is approximately 0.1 at 1 bar (Srečec et al. 1987), although there is evidence that this ratio decreases with increasing pressure (McCammon 1993; McCammon et al. 1998).

An important question to address, therefore, is how the solubility of Fe^{3+} may affect the thermodynamic properties and stability fields of iron-bearing mantle phases. Furthermore, as many studies have ignored the possible presence of Fe^{3+} and assumed that all Fe analysed with the electron microprobe was Fe^{2+}, these previous results may already include some unrecognised effect of Fe^{3+}. The Earth's mantle, however, probably contains quite low levels of Fe^{3+}, therefore a suitable approach is to first try to exclude Fe^{3+} altogether, or at least buffer it at the minimum concentration, and then to examine the effects when it is introduced.

Here, we report results from Fe–Mg partitioning experiments between ringwoodite and magnesiowüstite under conditions of metallic iron saturation and under more oxidising conditions using rhenium metal capsules. The Fe–Mg exchange equilibrium for these two phases can be written on a single-site basis as:

$$\underset{\text{ringwoodite}}{MgSi_{0.5}O_2} + \underset{\text{mw}}{FeO} = \underset{\text{ringwoodite}}{FeSi_{0.5}O_2} + \underset{\text{mw}}{MgO} \qquad (1)$$

Using these partitioning data we extract activity composition relations for the ringwoodite solid solution and $\Delta G^0_{(1)}$, the Gibbs free energy change for Eq. (1), by employing existing data for the mixing properties of the magnesiowüstite solid solution (Srečec et al. 1987). By performing these experiments in the presence of metallic Fe we ensure the minimum possible Fe^{3+} concentration in both phases. The effects of pressure and temperature on Eq. (1) are also examined.

Activity composition relations are necessary for constructing internally consistent phase diagrams involving the ringwoodite solid solution. Due to the difficulty in precise pressure control in the multianvil, it is difficult to determine the effect of small components such as Fe^{3+} on a phase boundary simply from phase equilibria experiments. If the effect on the thermodynamic properties of adding Fe^{3+} can be determined, however, then the influence on the phase boundaries can be calculated. In addition, the partitioning data collected over a range of pressures and temperatures can also be used to test the validity of other thermodynamic data such as those for the volume and entropy change of Eq. (1). The mixing properties determined for ringwoodite can in the future be used to determine similar properties for other solid solutions such as wadsleyite, pyroxene, akimotoite, garnet and $(Mg,Fe)SiO_3$ perovskite that coexist with ringwoodite.

Experimental methods

Synthetic $(Fe_xMg_{1-x})_2SiO_4$ olivines with $x = 0$, 0.2, 0.4, 0.6 and 0.8, were synthesised from analytical grade Fe_2O_3, MgO and SiO_2. Powders were ground together under alcohol then cold-pressed into pellets and sintered for 24 h in a CO–CO_2 gas mix furnace at 1200–1300 °C and at an f_{O_2} of approximately 1 log unit above the iron-wüstite (IW) buffer. Recovered samples were reground and resintered for a further 24 h. Samples were examined by powdered X-ray diffraction and no unreacted starting material remained. The lattice parameters were in agreement with those reported by Fisher and Medaris (1969) for the olivine solid solution. Magnesiowüstite $(Fe_xMg_{1-x})O$ powders with $x = 0.1$, 0.2, 0.4, 0.6 and 0.8 were kindly provided by S. Mackwell. These had been similarly prepared from Fe_2O_3 and MgO by sintering in a gas mix furnace under controlled f_{O_2} close to the IW buffer. Two suites of experimental starting compositions, with and without additional metallic Fe (≈10 mol%), were ground together from equimolar amounts of olivine and magnesiowüstite. Compositions of olivine and magnesiowüsitite were chosen such that they would approach the expected equilibrium composition from both higher and lower initial iron contents. Starting compositions are shown in Table 1.

Experiments were performed in a 500-tonne press using a Walker-type split-cylinder multianvil module (Walker et al. 1990). Experimental capsules were of either Re or Fe rod that was spark-eroded with multiple-sample chambers of 0.3 mm inside diameter. Rods of 1 and 1.5 mm outer diameter were eroded to give four to six sample chambers. Different starting materials could be loaded into each chamber and two such capsules could be run in a single experiment, allowing many compositions to be equilibrated at a given pressure and temperature. Starting materials loaded into Fe capsules always contained additional metallic Fe, while those in Re capsules contained no additional metal.

To pressures of 19 GPa a 10/5-type multianvil assembly was used, meaning that a 10-mm edge length Cr_2O_3-doped MgO octahedra was employed with tungsten carbide cubes of 5 mm truncation edge length. Above 19 GPa, a 7/3 type assembly was used. In both assemblies $LaCrO_3$ heaters were employed with W3%Re/W25%Re thermocouple. In the 10/5 assembly the thermocouple was

inserted axially inside an alumina tube and a single 1.5-mm capsule was used. In the 7/3 assembly the thermocouple passed horizontally through the walls of the furnace and two capsules were placed on either side of the thermocouple junction. Foils of Re were used to minimise Fe contamination to the thermocouple from the sample.

The pressure in the experiments was calibrated as shown in Fig. 1. Experiments were pressurised and then heated to desired temperatures between 1000 and 1600 °C within 2–3 min. Run durations were between 9 and 60 h, after which the experiments were quenched by switching off the power. In experiments employing Re capsules the temperature was controlled automatically and varied by less than ±5 °C from the set point while at high temperature. During the course of such experiments the electrical power varied very little (±5 W or 1% of the total power). When Fe capsules were used, contamination of the thermocouple by Fe in some experiments caused the apparent temperature to gradually drop, generally by about 100 °C. In these experiments the electrical power was kept constant at the level corresponding to that when the target temperature was first reached. The temperature uncertainty when thermocouple contamination occurred, estimated by comparing experiments where it did not occur, is considered to be ±20 °C at maximum. The recovered capsules were mounted in epoxy resin and carefully ground down such that the minimum of material was removed for all the sample chambers to be revealed. The top analysed surface of the section was consequently within approximately 30 μm of the thermocouple during the experiment, which should result in temperature uncertainties due to the thermal gradient of less than 20 °C. The polished samples were examined using micro-Raman spectroscopy and electron microprobe. Electron microprobe analyses were performed using a Cameca SX-50 operating at 15 kV and 15 nA. Standards were $MgSiO_3$ glass for Mg, andradite for Si and Fe metal. The data were reduced using the PAP correction routine.

Two samples (nos. 61 and 77) were made into petrographic thin sections for ion thinning and examination using analytical transmission electron microscopy (ATEM). The thin sections were glued on 3-mm-sized Mo grids and thinned to electron transparency by Ar ion bombardment under an incidence angle of 13° and at an acceleration voltage of 4.5 kV. TEM imaging, electron diffraction, energy-dispersive X-ray (EDX) and electron energy loss spectroscopy (EELS) were performed on a Philips CM20 FEG (field emission gun) STEM operating at 200 kV. The NORAN Vantage EDX system includes a digital pulse processor, a Ge detector and an ultrathin window, enabling the detection of light elements such as oxygen. EDX microanalyses were quantified according to the technique of Van Cappellen and Doukhan (1994), using the O *K* line as a measure of the sample thickness. Electron energy-loss near-edge structure (ELNES) spectra of the Fe *L*2, 3 edge were collected using a parallel electron energy-loss spectrometer (Gatan PEELS 666). Fe *L*2, 3 ELNES is a sensitive probe of the Fe^{3+}/Σ Fe ratio which, due to the high lateral resolution of a TEM, can be measured with a small electron probe (> 5 nm), enabling the separate acquisition of spectra of ringwoodite and magnesiowüstite in a mixed assemblage. ELNES spectra were collected in diffraction mode with convergence and collection semiangles of $\alpha = 8$ mrad and $\beta = 2.7$ mrad and an energy dispersion of 0.1 eV channel^{-1}.

Table 1 Starting compositions. Starting compositions used in Fe capsules had an additional 10 mol% metallic Fe, while compositions used in Re capsules had no added metal

Starting comp	Silicate Fe/(Fe + Mg)	Oxide Fe/(Fe + Mg)
A	0.0	0.20
B	0.10	0.40
C	0.20	0.10
D	0.20	0.60
E	0.40	0.40
F	0.40	0.80
G	0.60	0.60
H	0.80	0.80
I	0.60	0.80

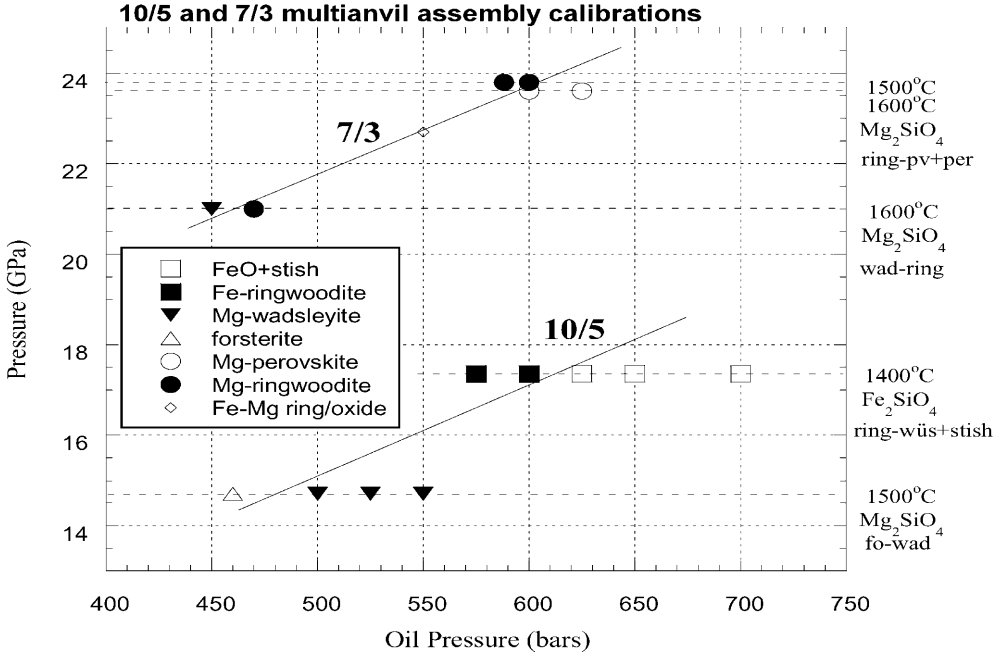

Fig. 1 Multianvil pressure calibrations for the 10/5 and 7/3 assemblies. The Walker-style module is used in a 500-tonne press, which has a ram diameter of 304.5 mm (1 bar = 0.73 tonnes). Calibrations were performed in the 10/5 assembly with the reaction of Mg_2SiO_4 forsterite to wadsleyite (Morishima et al. 1994) and Fe_2SiO_4 ringwoodite to wüstite plus stishovite (Katsura et al. 1998). The 7/3 assembly was calibrated using the Mg_2SiO_4 wadsleyite to ringwoodite transformation (Katsura and Ito 1989; Suzuki et al. 2000) and the reaction of Mg_2SiO_4 ringwoodite to $MgSiO_3$ perovskite plus periclase (Fei et al. 1990). The white diamond is determined from the Fe–Mg content of ringwoodite and magnesiowüstite in the presence of stishovite in experiment no. 78 using the data of Matsuzaka et al. (2000)

The width of the zero-loss peak at half height was ca. 0.8–0.9 eV. Quantification of spectra followed the procedure described by van Aken et al. (1998), using an empirically calibrated universal curve.

Results

Figure 2a shows a typical cross-section through the run products cut perpendicular to the long axis of the capsule. Each equilibrated sample was composed mainly of ringwoodite and magnesiowüstite, but in some Fe-poor compositions wadsleyite was observed and in some Fe-rich compositions in Re capsules stishovite also formed. The pressure range over which ringwoodite and magnesiowüstite can coexist is limited to below 23 GPa by the breakdown to silicate perovskite, and to pressures above 14 GPa due to the appearance of anhydrous

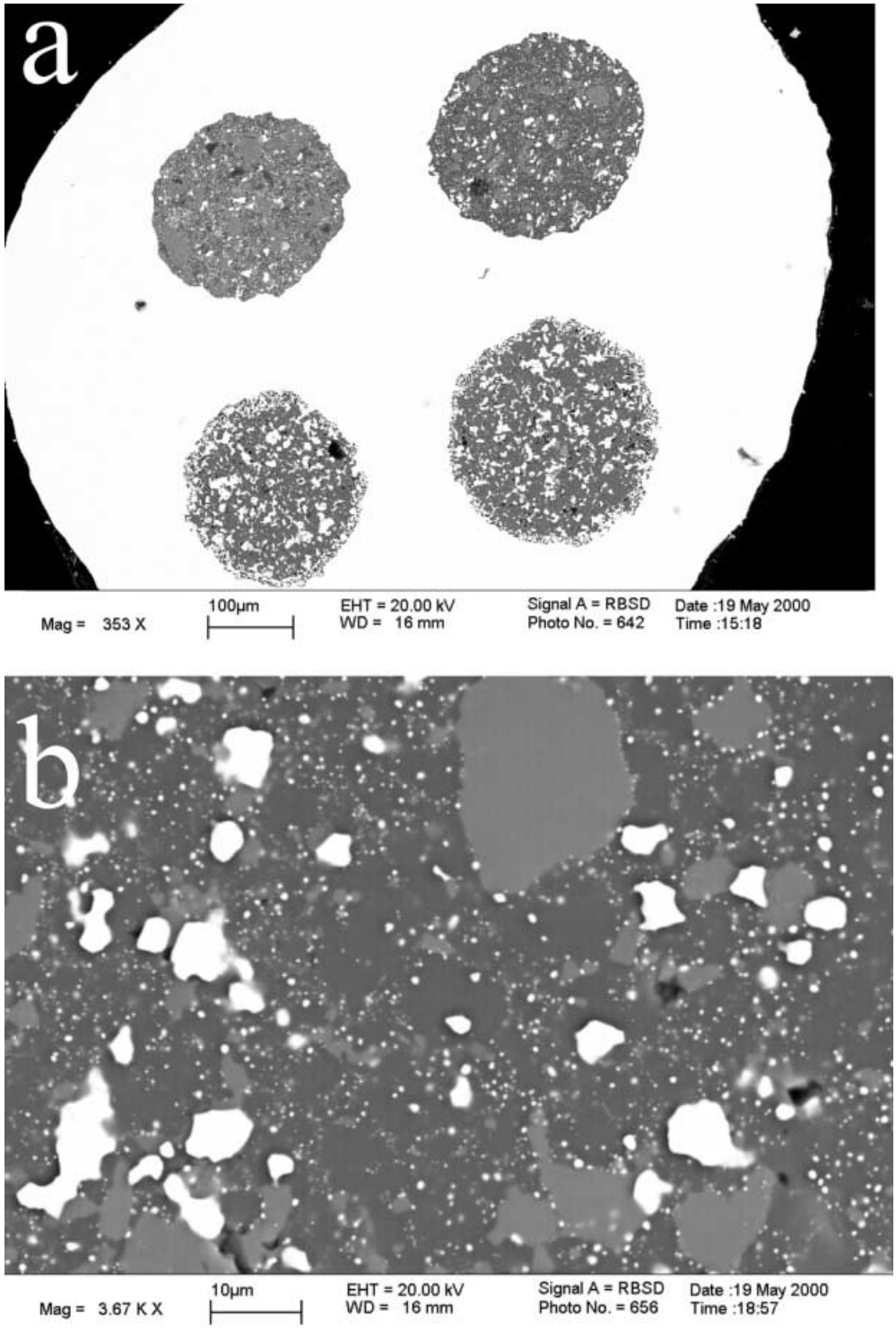

Fig. 2a Backscattered electron image of run products in an Fe capsule with four sample chambers. **b** Enlargement of the *top right sample chamber* in **a** showing darker ringwoodite and lighter magnesiowüstite grains surrounded by many small white grains of metallic Fe

phase B. Metallic Fe was present in all samples where it had been added (Fig. 2b); however, Mg-rich products often displayed a decrease in the metallic Fe content when compared to the starting composition and in some Fe-rich samples metallic Fe precipitated. Experiments performed in Re capsules with high bulk Fe contents also contained magnetite. TEM images of Fe-saturated experiments show well-crystallised grains of ringwoodite and magnesiowüstite with frequent metal particles on grain boundaries. The samples have usually developed a recrystallisation fabric with grain boundaries in textural equilibrium meeting at 120° angles (Fig. 3a, b). In line with this observation, dislocation densities were generally small or even undetectable. High concentrations of stacking faults in ringwoodite were common for low values of Fe/(Mg + Fe) (Fig. 3c), whereas high Fe/(Mg + Fe) ringwoodite was essentially free of stacking faults. Magnesiowüstite was also generally defect-free.

Between 10 and 20 pairs of electron microprobe analyses were made in each sample chamber, and these results are reported in Table 2. All Fe is reported here as FeO. Across each entire sample some variation in the Fe content occurred due to either reaction with the metallic Fe or uneven distribution of silicate and oxide grains. Fe contents within grains, however, showed little to no variation. Figure 4a shows all the microprobe analyses for one experiment and the average composition with one standard deviation (1σ) error bars. Although a range of Fe contents are observed for both phases within each sample, pairs of analyses of adjacent oxide and silicate fall along the general trend of the entire experiment, implying at least a local equilibrium between grains in each charge. Each pair of compositions has an uncertainty (1σ) calculated from the mean of the microprobe analyses for that sample. Due to the clear coupling of oxide and silicate analyses within individual samples, the uncertainties are likely to be slightly overestimated. The approach to equilibrium is also indicated in Fig. 4a. In some charges the oxide and silicate were both observed to decrease in Fe/(Fe + Mg).

Results for Fe–Mg partitioning between magnesiowüstite and ringwoodite in the presence of metallic Fe and in Re capsules are shown in Fig. 4b and c. Results in Fe capsules from various pressures and temperatures can be fitted to a single curve that passes within the experimental uncertainties of almost all the data, except some of the lower temperature points (1000–1200 °C). Results of partitioning in Re capsules show a marked difference from the Fe-saturated results over a similar range of pressure. For a given ringwoodite composition the equilibrium magnesiowüstite has a higher Fe content in Re than in Fe capsules. The two datasets are in good agreement for low Fe contents but start to diverge above ringwoodite Fe/(Fe + Mg) contents greater than 0.3. The maximum difference in magnesiowüstite Fe content for a given ringwoodite composition is approximately 8% between the Fe and Re capsule datasets.

In Fig. 4c a comparison is made with previous experimental data from Ito and Takahashi (1989), Fei et al. (1991) and Matsuzaka et al. (2000). There is apparently a greater effect resulting from the different capsule material used in these previous studies than from either the pressure or temperature variation. Fei et al. (1991) used molybdenum capsules, a quite reducing capsule material, and the results are in good agreement with the data from our study performed in the presence of metallic Fe. Ito and Takahashi (1989) and Matsuzaka et al. (2000) used tantalum and rhenium capsules, respectively, and these data are in good agreement with our experiments performed using rhenium capsules. Furthermore, the data of Matsuzaka et al. (2000) at 17 GPa are in perfect agreement with our results in Re capsules at 21 GPa, implying very little pressure effect on the partitioning but a much greater effect from the capsule material. Matsuzaka et al. (2000) performed one experiment in an Re capsule where they also added metallic Fe (5 wt%) to the sample. The result of this

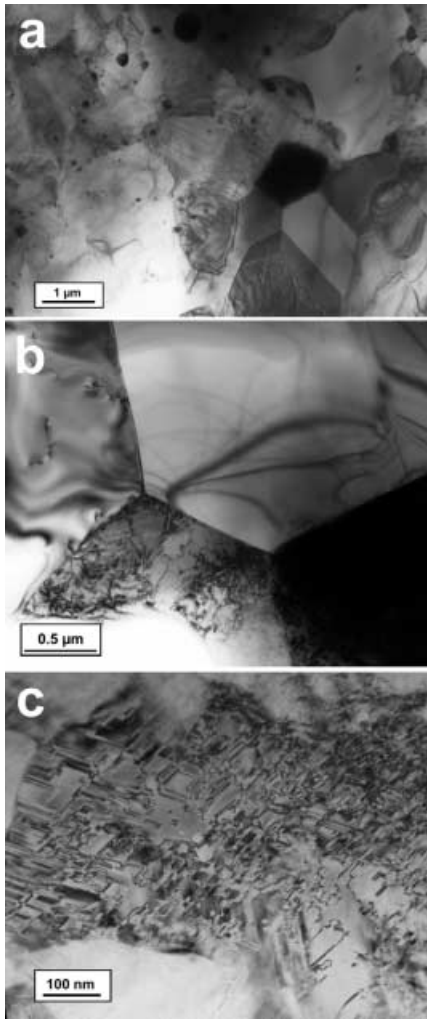

Fig. 3 **a** Bright-field TEM images of equilibrated samples showing coexisting ringwoodite, magnesiowüstite and metallic Fe grains. **b** Enlargement of **a** showing 120 ° triple junctions between two ringwoodite grains (*bottom* and *left*) magnesiowüstite (*top right*) and metallic Fe (*bottom right*). **c** A ringwoodite grain containing numerous stacking faults parallel to planes belonging to the {1 1 0} form

Table 2 Microprobe analyses of coexisting ringwoodite and magnesiowüstite**.** In the *left-hand column* are reported the run number, pressure, temperature, run duration, multianvil assembly and type of capsule used (Fe,Re) in each experiment. Uncertainties *in brackets* are in terms of least units cited

Exp. details	Start. comp	Ringwoodite					Magnesiowüstite			
		SiO_2 (wt%)	FeO (wt%)	MgO (wt%)	$\frac{Fe}{Fe+Mg}$		SiO_2 (wt%)	FeO (wt%)	MgO (wt%)	$\frac{Fe}{Fe+Mg}$
No. 49	B	40.91(22)	12.49(50)	48.08(38)	0.127(5)		0.07(7)	27.36(33)	73.7(12)	0.172(9)
23.5 GPa	E	40.66(12)	13.81(32)	47.14(20)	0.141(3)		0.07(7)	30.72(33)	70.57(30)	0.196(2)
1500 °C	D	39.18(14)	21.44(19)	40.98(17)	0.227(2)		0.02(1)	51.67(82)	50.25(60)	0.360(14)
10 h	G	39.62(38)	21.64(44)	40.56(54)	0.230(5)		0.06(6)	51.72(75)	49.8(11)	0.368(8)
7/3 Fe	A	41.12(22)	11.50(23)	48.43(20)	0.117(2)		0.07(10)	26.50(27)	74.28(27)	0.167(2)
	C	41.11(14)	11.75(23)	48.68(15)	0.119(2)		0.04(2)	26.77(24)	74.47(25)	0.168(1)
No. 50										
22 GPa	E	40.45(9)	14.37(20)	46.68(45)	0.147(3)		0.02(0)	31.82(75)	69.32(69)	0.205(5)
1500 °C	A	41.24(15)	10.04(29)	49.62(36)	0.102(3)		0.14(17)	22.24(57)	78.10(47)	0.138(4)
10 h	C	41.31(24)	10.11(25)	49.52(12)	0.103(2)		0.03(2)	22.47(47)	78.36(35)	0.139(3)
7/3 Fe	B	40.73(33)	11.78(47)	48.44(31)	0.120(5)		0.05(3)	24.21(85)	76.3(10)	0.155(1)
No. 61	E	36.77(32)	27.40(84)	36.01(75)	0.297 (9)		0.17 (30)	63.5 (18)	36.7(18)	0.490(19)
17.5 GPa	F	34.41(30)	39.69(56)	26.43(27)	0.456(4)		0.08(6)	81.64(65)	18.04(34)	0.715(4)
1400 °C	H	30.42(28)	57.75(27)	10.96(08)	0.745(2)		0.13(17)	93.74(57)	4.68(4)	0.918(1)
10 h	D	35.44(34)	32.7(18)	31.89(89)	0.363(14)		0.16(28)	71.7(17)	28.1(19)	0.587(22)
10/5 Fe	F	34.12(29)	39.92(56)	26.09(41)	0.460(7)		0.16(3)	82.00(80)	17.97(58)	0.717(8)
	G	34.08(11)	41.58(56)	25.07(29)	0.480(5)		0.05(5)	83.67(30)	16.61(37)	0.737(5)
	G	33.77(31)	42.96(40)	23.88(19)	0.500(4)		0.05(3)	84.85(46)	15.04(23)	0.758(3)
	C	40.14(34)	9.26(42)	50.69(35)	0.092(4)	wad	0.13(17)	28.80(13)	72.2(11)	0.181(9)
	B	38.08(41)	21.1(10)	41.34(10)	0.221(12)		0.10(15)	48.1(2)	52.5(24)	0.338(20)
	D	35.83(39)	32.2(12)	32.68(68)	0.354(13)		0.26(50)	71.3(16)	29.4(13)	0.574(17)
	I	33.26(43)	45.0(66)	22.14(48)	0.531(8)		0.08(13)	86.87(57)	13.00(51)	0.788(7)
No. 62	A	40.00(36)	11.14(37)	48.93(28)	0.112(3)		0.08(10)	24.3(13)	76.43(77)	0.150(7)
21.5 GPa	G	39.71(35)	15.73(20)	45.50(19)	0.161(2)		0.15(22)	35.11(39)	65.79(57)	0.229(3)
1500 °C	F	39.41(5)	15.16(10)	46.27(27)	0.154(2)		0.14(11)	36.1(26)	66.56(10)	0.232(6)
9 h	C	40.02(22)	10.24(23)	49.21(16)	0.104(2)		0.90(47)	22.16(66)	77.0(13)	0.138(4)
7/3 Fe	B	39.61(34)	12.01(57)	48.07(22)	0.123(5)		0.28(25)	26.02(99)	73.39(59)	0.165(6)
	E	39.01(21)	14.64(39)	46.43(26)	0.150(3)		0.59(42)	31.88(81)	68.09(66)	0.205(5)
	D	40.01(33)	14.44(04)	45.88(28)	0.149(1)		0.12(2)	33.9(17)	67.99(53)	0.216(10)
No. 63	E	38.23(27)	23.66(41)	38.92(46)	0.253(6)		0.16(34)	52.98(17)	46.8(15)	0.386(15)
17.5 GPa	B[a]	39.46(25)	15.95(91)	45.24(59)	0.158(5)	wad	0.05(5)	50.05(14)	50.8(15)	0.354(13)
1600 °C	B	38.49(20)	21.79(40)	40.56(49)	0.230(9)		0.05(5)	50.05(14)	50.8(15)	0.354(13)
10 h	G	35.42(32)	38.1(11)	27.64(65)	0.432(12)		0.09(10)	79.47(15)	20.6(13)	0.681(18)
10/5 Fe	F	35.71(22)	35.40(30)	29.86(25)	0.398(3)		0.10(11)	76.10(53)	24.34(25)	0.635(3)
	D	37.09(47)	27.17(70)	36.32(45)	0.294(7)		0.04(1)	61.15(12)	39.3(12)	0.463(13)
No. 64	C[a]	40.67(24)	5.77(75)	53.10(33)	0.057(7)	wad	0.08(7)	22.74(12)	75.7(13)	0.143(8)
17.5 GPa	B	38.12(60)	18.92(12)	42.73(62)	0.197(12)		0.63(55)	42.32(18)	57.1(16)	0.290(22)
1200 °C	E	37.19(19)	26.42(46)	37.01(14)	0.284(4)		0.19(24)	64.46(10)	36.4(10)	0.496(11)
22 h	I	33.55(28)	43.98(61)	22.96(24)	0.516(5)		0.40(38)	86.29(90)	13.26(33)	0.783(6)
10/5 Fe	F	34.41(49)	39.84(66)	26.58(14)	0.454(5)		0.33(22)	82.88(97)	17.09(41)	0.729(7)
	H	30.88(24)	58.02(49)	10.90 (9)	0.747(2)		0.07(6)	94.48(75)	4.48(9)	0.921(2)
No. 66	G	34.70(24)	42.83(98)	23.64(27)	0.500(9)		0.25(13)	85.71(70)	14.26(62)	0.770(9)
11 GPa	I	33.96(60)	45.60(66)	21.26(37)	0.545(8)		0.19(3)	88.25(32)	11.25(14)	0.813(2)
1000 °C	F	35.39(35)	38.96(43)	27.15(38)	0.444(5)		0.37(25)	82.15(12)	17.00(46)	0.729(8)
60 h										
No. 67	B	39.96(32)	14.69(66)	46.54(38)	0.149(7)		0.26(23)	31.35(63)	69.1(10)	0.201(6)
21.5 GPa	D	39.99(30)	17.07(45)	43.86(37)	0.178(4)		0.32(24)	38.74(36)	60.9(15)	0.261(7)
1600 °C	E	37.26(22)	20.49(57)	43.22(93)	0.208(10)		0.04(1)	43.9(13)	57.24(55)	0.294(8)
9 h	C	40.97(18)	12.90(66)	47.19(42)	0.132(6)		0.11(6)	28.73(83)	71.28(96)	0.183(6)
7/3 Fe	A	40.80(26)	12.66(34)	46.50(32)	0.131(4)		0.40(63)	27.7(1)	70.5(21)	0.179(11)
No. 68	I	39.15(90)	30.33(20)	32.75(99)	0.343(4)		0.03(2)	69.41(12)	30.75(26)	0.556(2)
21 GPa	E	39.16(15)	21.64(36)	40.67(21)	0.228(4)		0.04(3)	50.70(87)	50.57(53)	0.358(6)
1600 °C	C	39.09(28)	20.40(96)	42.19(69)	0.212(11)		0.22(18)	45.08(64)	55.83(35)	0.310(13)
8 h	B	39.25(29)	20.64(39)	41.86(30)	0.215(3)		0.03(2)	46.81(74)	54.60(55)	0.323(5)
10/5 Fe	F	37.67(25)	29.17(89)	34.71(75)	0.318(11)		0.25(48)	65.78(95)	34.66(71)	0.513(20)
	H	36.57(16)	33.80(44)	30.73(26)	0.379(4)		0.03(1)	74.61(56)	25.44(62)	0.620(7)
No. 77	G	37.58(41)	30.12(69)	34.48(49)	0.329(6)		1.08(5)	74.84(54)	22.78(65)	0.647(8)
22.7 GPa	G[a]					mag	2.09(12)	82.05(65)	8.81(28)	0.839(4)
1600 °C	B	39.8(14)	16.16(98)	45.50(83)	0.166(12)		0.37(14)	39.6(16)	60.4(16)	0.273(27)
10 h	A	40.96(29)	13.67(37)	47.12(45)	0.139(4)		0.18(2)	33.5(10)	67.1(10)	0.217(7)

Table 2 (Continued)

Exp. details	Start. comp	Ringwoodite					Magnesiowüstite			
		SiO_2 (wt%)	FeO (wt%)	MgO (wt%)	$\frac{Fe}{Fe+Mg}$		SiO_2 (wt%)	FeO (wt%)	MgO (wt%)	$\frac{Fe}{Fe+Mg}$
7/3 Re	D	38.44(10)	26.45(28)	37.30(18)	0.283(2)		0.97(3)	69.05(44)	29.04(31)	0.569(4)
	I	37.3(26)	38.9(13)	25.8(10)	0.456(3)		1.13(16)	83.89(32)	12.62(29)	0.787(4)
	I[a]					mag	2.73(32)	83.58(78)	6.02(05)	0.885(1)
	E	38.68(27)	25.52(34)	37.85(35)	0.273(4)		0.63(3)	65.69(91)	33.13(97)	0.524(11)
	G	41.08(45)	13.2(19)	47.2(14)	0.135(20)		0.20(4)	32.8(49)	67.2(49)	0.214(37)
	F	36.81(15)	34.17(46)	30.95(24)	0.380(4)		0.98(7)	79.46(56)	17.87(32)	0.712(5)
No. 81	A	42.28(44)	6.79(15)	50.50(36)	0.07(3)		0.06(2)	14.94(4)	83.30(32)	0.090(1)
21 GPa	B	40.72(21)	13.12(15)	47.91(18)	0.13(1)		0.15(11)	30.83(58)	70.37(49)	0.196(4)
1600 °C	E	38.98(52)	24.64(25)	37.81(81)	0.27(4)		0.23(5)	62.18(29)	37.79(23)	0.478(2)
10 h	D	36.79(35)	28.93(29)	35.29(16)	0.31(2)		0.22(2)	71.43(44)	29.35(16)	0.575(2)
7/3 Re	G	36.42(95)	33.18(62)	31.71(31)	0.37(4)		0.40(5)	78.46(44)	20.74(33)	0.676(5)
	F	37.21(82)	33.81(54)	30.28(48)	0.38(4)		0.43(2)	79.45(58)	19.51(25)	0.694(2)
	F[a]					mag	0.51(10)	84.75(34)	13.57(18)	0.779(13)
	C	41.07(48)	9.16(31)	48.89(19)	0.09(2)		0.30(28)	20.83(32)	76.98(47)	0.132(2)

[a] Reported analyses are for either magnetite (*mag*) reported on right or wadsleyite (*wad*) reported on left

experiment is close to other results from Re capsules where Fe was not added. The fact that the presence of metal did not appear to affect the partitioning in this experiment is puzzling, but this may be because insufficient metallic Fe was added to buffer the oxygen fugacity throughout this sample.

The electron microprobe analyses also detected SiO_2 in magnesiowüstite as shown in Fig. 5a. In Fe capsules the SiO_2 content is apparently not coupled with Fe/(Fe + Mg) and is generally below 0.4 wt%. These contents are at the limit of the microprobe detection and the occasional higher values are probably due to small amounts of beam overlap with adjacent ringwoodite or stishovite grains. In Re capsules, however, SiO_2 contents are greater and increase with the Fe content, reaching a maximum of approximately 1.1 wt%. Magnetite found in Re capsules also contains between 2 and 3 wt% of SiO_2. Energy-dispersive analyses using the TEM also confirmed that larger amounts of SiO_2 were present in magnesiowüstite formed in Re capsules than in Fe capsules. Measurements made using the TEM showed that the analysed grains were inclusion-free and that the SiO_2 was indeed soluble in the structure of magnesiowüstite produced at high pressure in Re capsules. The solubility mechanism of Si^{4+} in magnesiowüstite is not clear, but as the SiO_2 content is apparently coupled to the Fe^{3+} content, the mechanism might involve forming stable clusters of Si^{4+}, Fe^{3+} and vacancies. The solubility of Si^{4+} in magnesiowüstite was observed to decrease with pressure.

The Fe^{3+}/Σ Fe contents of magnesiowüstite, ringwoodite and wadsleyite were determined on the basis of Fe $L2,3$ ELNES spectra like those shown in Fig 6. Experiments no. 61 and no. 77 were ion-thinned and several samples within each capsule were analysed. Figure 5b shows the EELS results for $Fe^{3+}/\Sigma Fe$ in Re and Fe capsules. For each measurement the Fe/(Fe + Mg) content was simultaneously measured using the EDX analyser on the TEM. In Fe capsules $Fe^{3+}/\Sigma Fe$ contents in ringwoodite and magnesiowüstite are generally below 0.1. The Fe^{3+} content for both phases increases with increasing bulk Fe content and for a given bulk Fe content ringwoodite appears to contain slightly more Fe^{3+}. For Fe/(Fe + Mg) contents less than 0.6 the $Fe^{3+}/\Sigma Fe$ measurements for both ringwoodite and magnesiowüstite are below 0.05, which is effectively zero within the uncertainty of the technique. The results for wadsleyite, however, show quite high Fe^{3+} concentrations and although these measurements were made within one sample, they vary over a significant range of Fe^{3+}. These high Fe^{3+} levels and the scattering of the analyses are not due to electron-beam damage of the sample because the peaks arising from Fe were not observed to change with exposure time to the beam. If the wadsleyite crystals in the sample were in equilibrium with metallic Fe we would expect a single value of Fe^{3+} content varying only with the MgO content. The most likely explanation, therefore, is that equilibrium between the silicate and metallic Fe in this sample was not achieved. This might be due to the relatively low amount of metallic Fe remaining dispersed throughout this particular sample and to the fact that the area thinned for investigation was in the centre of the sample and away from the Fe wall of the capsule. This implies, however, that the Fe capsule wall, being only a maximum of 150 μm away from any part of the sample, had little influence over the Fe^{3+} concentration in the centre of the charge, despite a run duration of 10 h at 1400 °C. The additional oxygen in the wadsleyite may have been present in magnesiowüstite in the starting composition or may have come from trapped pore space or could have diffused into the sample chamber from outside the capsule. These results suggest, however, that placing samples in Fe capsules, without also including metal powder in the sample, may not be sufficient to buffer all the material at conditions close to IW. We cannot assess whether equilibrium was achieved for Fe^{3+} contents in ringwoodite–magnesiowüstite experiments, as the Fe^{3+}

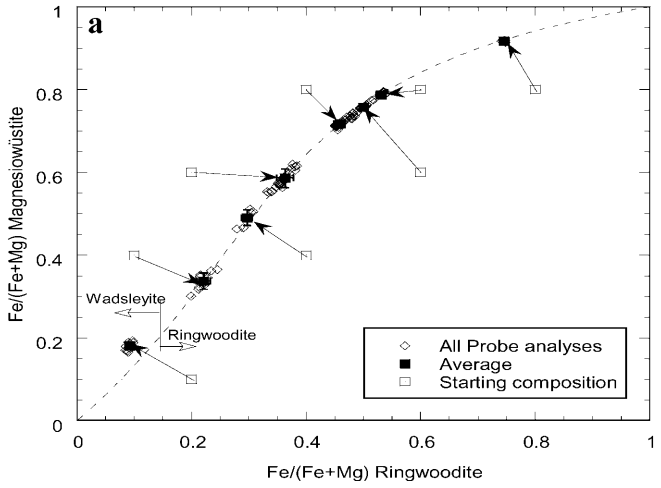

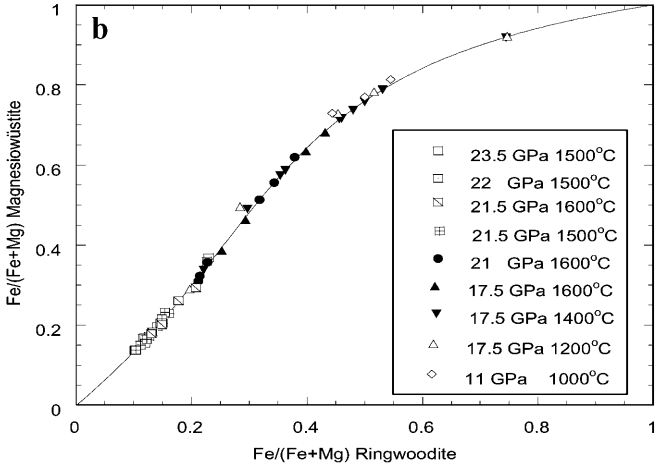

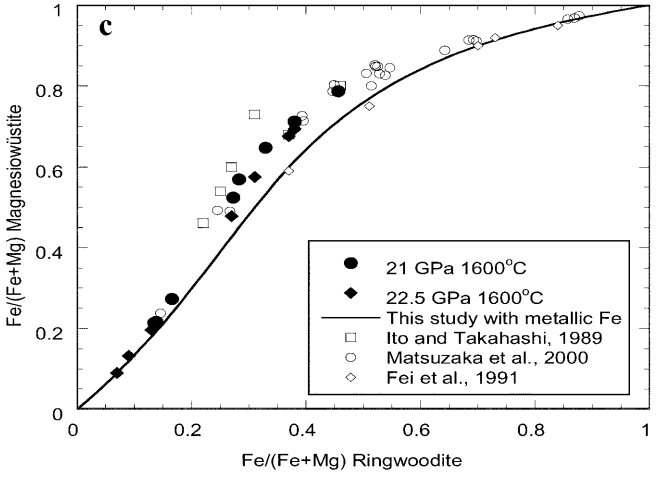

Fig. 4a–c Results of Fe–Mg partitioning between ringwoodite and magnesiowüstite in the presence of metallic Fe and in Re capsules. **a** The approach to equilibrium is shown for an experiment at 17.5 GPa and 1400 °C at metallic Fe saturation. *Open squares* denote starting compositions, and the microprobe analyses, with all Fe reported as FeO, are shown as *open diamonds*. The average compositions with 1σ uncertainties are shown. **b** Results from partitioning at various pressures and temperatures in the presence of metallic Fe. **c** Results of partitioning experiments performed in Re capsules are compared with the best-fit line for the Fe-saturated experiments and results from Ito and Takahashi (1989), Fei et al. (1991) and Matsuzaka et al. (2000)

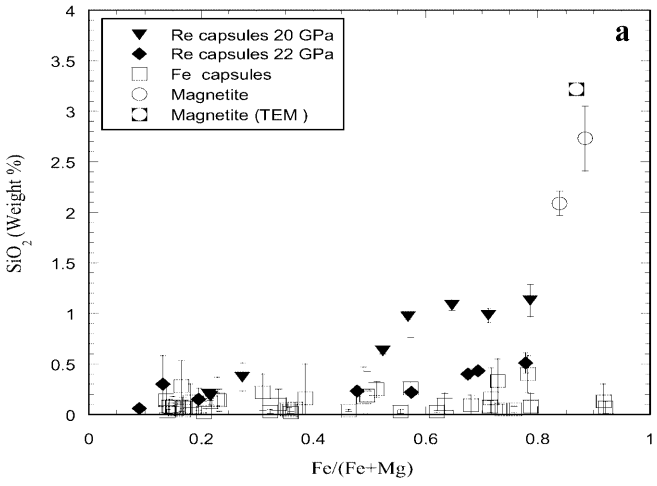

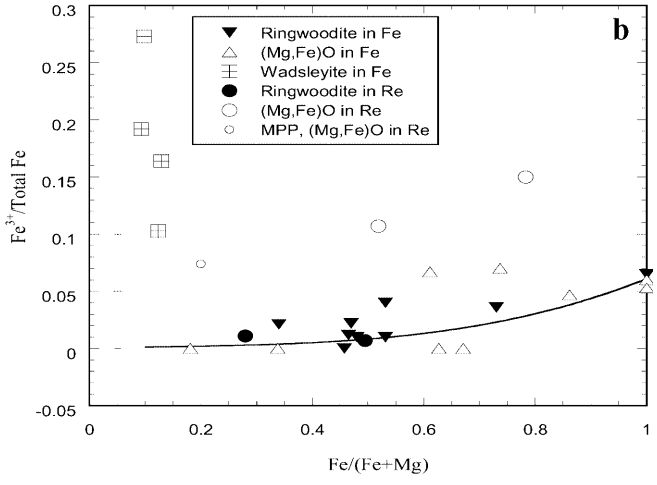

Fig. 5 a The concentration of SiO_2 in magnesiowüstite measured using the electron microprobe. **b** Fe^{3+} concentrations in ringwoodite and magnesiowüstite determined from Fe *L*2,3 ELNES spectra. End-member Fe compositions were determined by X-ray diffraction analyses using the unit cell-Fe^{3+} calibrations of Simons (1980) for magnesiowüstite and O'Neill et al. (1993) for ringwoodite. The uncertainty in $Fe^{3+}/\Sigma Fe$ for ELNES and X-ray data is 0.05, as shown in the *bottom left corner* of the diagram. Results for wadsleyite are most likely not in equilibrium with metallic Fe. MPP refers to McCammon et al. (1998). The best estimate curve for the Fe^{3+} concentration at Fe saturation in ringwoodite and magnesiowüstite is shown (see text for details)

contents were not reversed. However, the consistency of these measurements and the similarity of the magnesiowüstite Fe^{3+} concentrations with those measured at Fe saturation at 1 bar (Srečec et al. 1987) make us quite confident that Fe^{3+} equilibrium was achieved.

In Re capsules Fe^{3+} concentrations of magnesiowüstite are approximately three times higher for a given bulk Fe content than in Fe capsules. The coexisting ringwoodite appears to contain very little Fe^{3+} over the measured compositional range. It is interesting to note that the highest Fe^{3+} content for magnesiowüstite in Re is for a sample that also contains magnetite. The Fe^{3+} content is, however, approximately half the concentration observed for magnesiowüstite coexisting with magnetite at 1 bar (Speidel 1967) and the Fe^{3+} content of

coexisting ringwoodite is effectively zero. This difference in Fe^{3+} partitioning between the Fe oxides could be evidence that magnetite in these samples was transformed to a high-pressure polymorph, possibly a $CaMn_2O_4$-type or $CaTi_2O_4$-type structure, as previously observed in diamond anvil cell experiments (Fei et al. 1999; Haavik et al. 2000), but backtransformed to magnetite on return to room pressure. A similar explanation was proposed by McCammon et al. (1998), who also observed lower Fe^{3+} contents for magnesiowüstite formed at high pressure and relatively oxidising conditions when compared to 1-bar measurements. Our TEM observations reveal that the magnetite contains numerous polysynthetic twins parallel to (3 1 1), which may be a further indication that a back-transformation has occurred (Fig. 7).

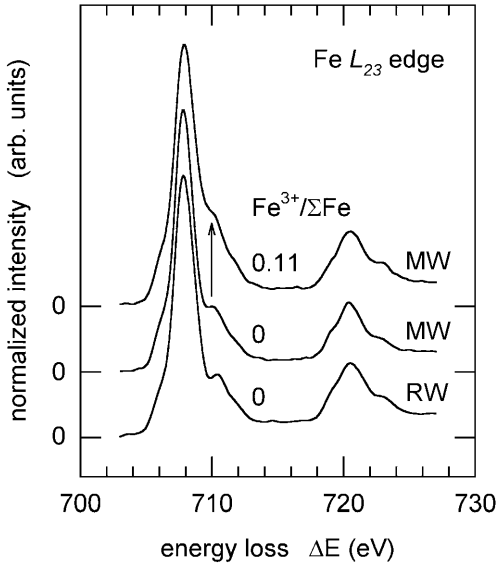

Fig. 6 Typical Fe *L*2,3 ELNES of magnesiowüstite (*MW*) and ringwoodite (*RW*). The spectra have been normalised to their maximum intensity and shifted vertically for clarity. Note the variation in the intensity of the peak at ca. 710 eV, reflecting the variation in the Fe^{3+} contents of MW as indicated by an *arrow*. Spectra have been gain-normalised, background-subtracted and deconvoluted using the low-loss spectra, and the $Fe^{3+}/\Sigma Fe$ has been determined by the treatment described by van Aken et al. (1998)

Discussion

The two types of capsules used in these experiments clearly impose different oxygen fugacities, which influences the Fe^{3+} content of the phases and the apparent Fe–Mg partitioning. The oxygen fugacity imposed by Fe saturation is lower than in Re capsules and, as the EELS data show, the Fe^{3+} concentration is lower in samples equilibrated in Fe capsules than in Re capsules. The oxygen fugacity (f_{O_2}) of the experiments performed in the presence of metallic Fe can be calculated from the equilibrium

$$\underset{\text{metal}}{Fe} + 0.5O_2 = \underset{\text{mw}}{FeO} \quad . \tag{2}$$

f_{O_2} varies in each sample as the activity of FeO is lowered due to the solution of MgO. The range of f_{O_2} for a typical sample calculated at 21 GPa and 1600 °C is between IW and IW − 1.4. The Re–ReO_2 buffer under the same conditions, however, is IW + 5.5 (Pownceby and

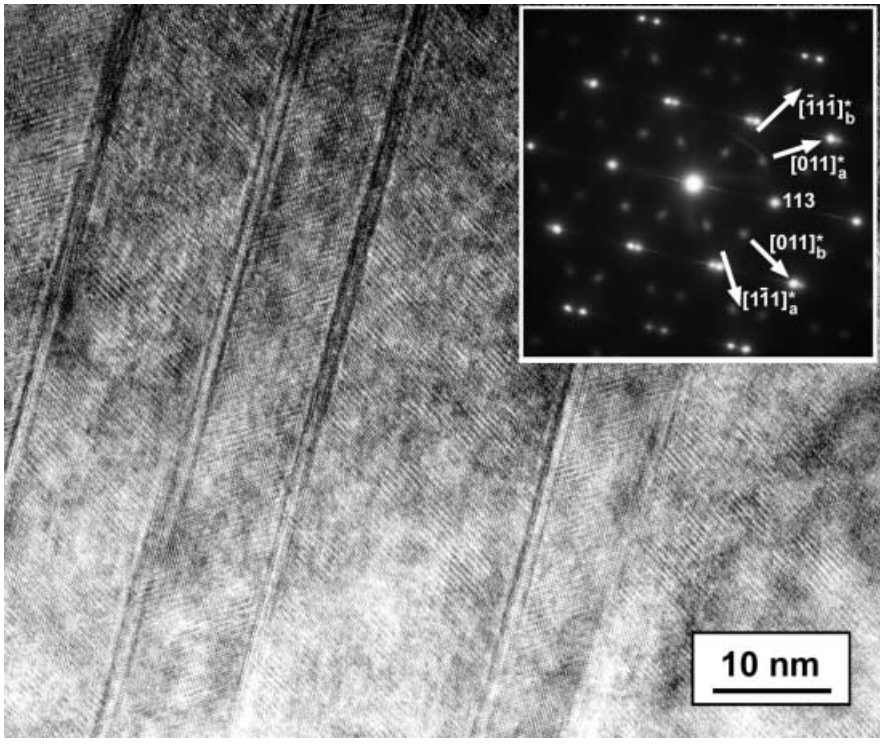

Fig. 7 High-resolution TEM image of polysynthetic twinning in magnetite from experiment no. 77. Twins are parallel to (3 1 1) and may result from a retrograde transformation from a high-pressure structure

O'Neill 1994), although this is a maximum estimate for the oxygen fugacity in Re capsules because ReO_2 was not added or detected in any of the experiments. For the Re–ReO_2 buffer there is also little available equation of state data. As magnetite appears with magnesiowüstite in experiment no. 77 the oxygen fugacity can also be calculated, using data from O'Neill (1988) and the reaction

$$\underset{\text{mw}}{3FeO + 0.5O_2} = \underset{\text{magnetite}}{Fe_3O_4} \quad . \tag{3}$$

The activities of FeO and Fe_3O_4 must be adjusted to account for the MgO content. The calculated f_{O_2} at 1600 °C and 21 GPa is approximately IW + 8.5, which is three log units higher than Re–ReO_2 under these conditions. Even considering significant uncertainties, this still suggests that in these experiments either Re should oxidise or magnetite should be reduced. The coexistence of Re and magnetite is therefore strong evidence that magnetite goes through a high-pressure phase transformation. If we correct only the volume of magnetite for the 6.5% volume change suggested for the magnetite to $CaMn_2O_4$-type phase transformation (Fei et al. 1999), then the f_{O_2} for Eq. (3) becomes IW + 6, which is well within the uncertainties of the Re–ReO_2 buffer under these conditions.

Measurements made on peridotite xenoliths imply that the upper mantle has a quite low $Fe^{3+}/\Sigma Fe$ ratio, which has been estimated to be approximately 0.02 (O'Neill et al. 1993). Fe^{3+} is mainly dissolved in minerals of lower modal abundance in the upper mantle such as spinel, clinopyroxene and garnet due to the low solubility of Fe^{3+} in olivine. Because Fe^{3+} component activities are consequently high in these minor minerals, the resultant oxygen fugacity is also relatively high and is generally within −1.5 to +0.5 log units of the quartz–fayalite–magnetite oxygen buffer (ΔQFM = −1.5 to 0.5), as revealed by oxygen thermobarometry measurements. The f_{O_2} of the Re–ReO_2 buffer is quite close to QFM under these conditions and, consequently, Re capsules impose oxygen fugacities that are realistic for the upper mantle. However, at higher pressures Fe^{3+} becomes increasingly more soluble in dominant mantle minerals such as wadsleyite, ringwoodite, majoritic garnet and silicate perovskite. Fe^{3+} component activities in these phases will then be lower because Fe^{3+} is more dilute in these dominant mantle phases and the oxygen fugacity will be consequently also lower. If the $Fe^{3+}/\Sigma Fe$ ratio estimated for the upper mantle remains constant, then the transition zone and lower mantle are likely to be at an oxygen fugacity closer to the IW buffer than to QFM. Experiments at metallic Fe saturation are therefore likely to be more applicable to the deeper mantle than experiments at higher oxygen fugacities in Re capsules.

Activity–composition relations

From the partitioning data we can extract thermodynamic parameters to describe the non-ideal mixing of ringwoodite and determine the free energy change, $\Delta G^0_{(1)}$, for Eq. (1). By using the data collected at Fe saturation we ensure the lowest possible Fe^{3+} concentration and we are, therefore, closer to the oxidation conditions likely to occur in the transition zone and lower mantle of the Earth. Although we have made measurements of Fe^{3+} concentrations at high and low oxygen fugacities, we do not have enough accurate data on Fe^{3+} variation to derive a ternary mixing model for the partitioning between the two phases. We can, however, treat the data collected at metallic Fe saturation with binary Fe^{2+}–Mg^{2+} mixing rules and make a small correction for the presence of Fe^{3+} in the bulk Fe analyses.

At metallic Fe saturation it is assumed that both magnesiowüstite and ringwoodite have maximum $Fe^{3+}/\Sigma Fe$ contents of approximately 0.06 that occur in the Fe-rich end members. The Fe^{3+} concentration in both phases is then assumed to vary with Fe/(Fe + Mg) along a curve of the same shape as that determined by Srečec et al. (1987) for magnesiowüstite at 1 bar. The proposed curve for the Fe^{3+}contents of both phases at Fe saturation is shown in Fig. 5b. This results in an Fe^{3+} distribution coefficient between the two phases ($K^{\text{ring/mw}}_{D_{Fe^{3+}}}$) that can be described by the equation $K^{\text{ring/mw}}_{D_{Fe^{3+}}} = 1.6\text{–}3.92X^{\text{mw}}_{FeO} + 2.96X^{\text{mw}^2}_{FeO}$ over the range of experimental compositions at Fe saturation. The conditions for equilibrium of Eq. (1) can be written as follows:

$$\Delta G^0_{(1)} = -RT \ln \frac{a^{\text{mw}}_{MgO} a^{\text{ring}}_{FeSi_{0.5}O_2}}{a^{\text{ring}}_{MgSi_{0.5}O_2} a^{\text{mw}}_{FeO}} \quad , \tag{4}$$

where $\Delta G^0_{(1)}$ is the free energy change of Eq. (1) at the pressure and temperature of interest. For magnesiowüstite the activities are expressed as:

$$a^{\text{mw}}_{MgO} = X^{\text{mw}}_{MgO} \cdot \gamma^{\text{mw}}_{MgO} \tag{5}$$

$$a^{\text{mw}}_{FeO} = X^{\text{mw}}_{FeO} \cdot \gamma^{\text{mw}}_{FeO} \quad , \tag{6}$$

where, for example:

$$X^{\text{mw}}_{FeO} = \left(\frac{Fe^{2+}}{Fe^{2+} + Fe^{3+} + Mg^{2+}} \right) \quad . \tag{7}$$

For ringwoodite we assume Fe^{3+} is completely disordered over both octahedral and tetrahedral sites, such that:

$$a^{\text{ring}}_{FeSi_{0.5}O_2} = (X^{\text{ring}}_{Fe} \cdot \gamma^{\text{ring}}_{Fe})(X^{\text{ring}}_{Si} \cdot \gamma^{\text{ring}}_{Si})^{0.5} \quad . \tag{8}$$

As the amount of Fe^{3+} mixing on the tetrahedral site is small (<2%) it can be ignored and Eq. (8) simplifies to:

$$a^{\text{ring}}_{FeSi_{0.5}O_2} = (X^{\text{ring}}_{Fe} \cdot \gamma^{\text{ring}}_{Fe}) \tag{9}$$

with

$$X^{\text{Ring}}_{Fe} = \frac{Fe^{2+}}{Fe^{3+}_{\text{oct}} + Fe^{2+} + Mg^{2+}} \quad . \tag{10}$$

The Fe^{2+}–Mg^{2+} partition coefficient (K_D) or equilibrium coefficient for Eq. (1) is:

$$K_D = \frac{X^{mw}_{MgO} X^{ring}_{Fe}}{X^{ring}_{Mg} X^{mw}_{FeO}} \quad (11)$$

and Eq. (4) can be rewritten as:

$$\Delta G^0_{(1)} = -RT \ln K_D - RT \ln \frac{\gamma^{mw}_{MgO}\gamma^{ring}_{FeSi_{0.5}O_2}}{\gamma^{ring}_{MgSi_{0.5}O_2}\gamma^{mw}_{FeO}} \quad . \quad (12)$$

Making the assumption that both solid solutions are non-ideal but can be described as regular symmetric solutions, then two interaction parameters can be written for each solid solution, i.e

$$RT \ln \gamma^{mw}_{MgO} = W^{mw}_{FeMg}(1 - X^{mw}_{MgO})^2 \quad (13)$$

$$RT \ln \gamma^{mw}_{FeO} = W^{mw}_{FeMg}(1 - X^{mw}_{FeO})^2 \quad , \quad (14)$$

where W^{mw}_{FeMg} is a symmetric interaction parameter. Two similar equations can be written for ringwoodite. Substituting Eqs. (13) and (14) and their ringwoodite equivalents into Eq. (12) and rearranging gives the expression:

$$\begin{aligned} RT \ln K_D &= -\Delta G^0_{(1)} - W^{mw}_{FeMg}(1 - X^{mw}_{MgO})^2 - W^{ring}_{FeMg}(1 - X^{ring}_{Fe})^2 \\ &\quad + W^{mw}_{FeMg}(1 - X^{mw}_{FeO})^2 + W^{ring}_{FeMg}(1 - X^{ring}_{Mg})^2 \quad . \end{aligned} \quad (15)$$

$\Delta G^0_{(1)}$ is a constant at fixed pressure and temperature. Fitting data from experiment no. 61 performed at 1400 °C and 17.5 GPa to Eq. (15) by means of a weighted least-squares regression gives values for W^{ring}_{FeMg} and W^{mw}_{FeMg} of 0.7 (5) and 9.3 (5) kJ mol^{-1}, respectively, and a $\Delta G^0_{(1)}$ of 11.0 kJ mol^{-1}. If the Fe^{3+} contents are ignored, the fit gives $W^{ring}_{FeMg} = 1.0$ kJ mol^{-1}, $W^{mw}_{FeMg} = 9.7$ kJ mol^{-1} and $\Delta G = 10.9$ kJ mol^{-1}. As the inclusion of Fe^{3+}has a quite small effect on the calculation, the uncertainty in the Fe^{3+}concentration and the assumptions made about the site occupancy of Fe^{3+}in ringwoodite will not significantly affect the results. Uncertainties in K_D were propagated from the compositional error with the equation

$$\sigma_{K_D} = \sqrt{\left[\frac{\sigma^{mw}_{FeO}}{X^{mw}_{FeO}(1 - X^{mw}_{FeO})}\right]^2 + \left[\frac{\sigma^{ring}_{Fe}}{X^{ring}_{Fe}(1 - X^{ring}_{Fe})}\right]^2} \quad . \quad (16)$$

The three values determined by simple fitting of Eq. (15) are highly correlated and a range of both parameters can adequately fit the correctly weighted partitioning data. If W^{mw}_{FeMg} is increased and the other two parameters are then refined, we find that the three values that still fit the uncertainties are $W^{ring}_{FeMg} = 5.4$ kJ mol^{-1}, $W^{mw}_{FeMg} = 15$kJ mol^{-1} and $\Delta G^0_{(1)} = 8.2$ kJ mol^{-1}. Similarly, if W^{ring}_{FeMg} is lowered, then values of $W^{ring}_{FeMg} = 0$ kJ mol^{-1}, $W^{mw}_{FeMg} = 8.2$ kJ mol^{-1} and $\Delta G^0_{(1)} = 11.4$ kJ mol^{-1} still fit within the uncertainties. The three parameters are therefore only constrained to within 5–6 kJ mol^{-1}. The difference between the interaction parameters ($W^{mw}_{FeMg} - W^{ring}_{FeMg}$) is, however, quite well constrained by the data to be approximately 8.5 kJ mol^{-1}. If a similar procedure is followed with the data from Re capsules, the determined value for $W^{mw}_{FeMg} - W^{ring}_{FeMg}$ is 12.7 kJ mol^{-1}; this value, however, makes no allowance for the significant amount of Fe^{3+} in magnesiowüstite under these conditions.

As the results from this type of analysis are strongly correlated, either $\Delta G^0_{(1)}$ or W^{mw}_{FeMg} must first be known in order to calculate meaningful ringwoodite mixing properties. Values of $\Delta G^0_{(1)}$ at pressure and temperature probably cannot optimistically be estimated to better than 5 kJ mol^{-1} with current equation of state and calorimetric data. Activity composition relations for the magnesiowüstite solid solution, however, have been measured at metallic Fe saturation at 1 bar (Srečec et al. 1987). These measurements, made between 777 and 1130 °C, also include measurements of the Fe^{3+} content of magnesiowüstite. In this previous study, asymmetric Margules-type equations are given for the activity coefficients of FeO, $Fe_{2/3}O$ and MgO as a function of magnesiowüstite composition. The data of Srečec et al. (1987) can be extrapolated to higher pressures using excess molar volume data for the solid solution and using the expression:

$$RT \ln \gamma_{i,1bar} = RT \ln \gamma_{i,P} + \int_1^P \bar{V}_i - V^0_i \, dP \quad , \quad (17)$$

where $\bar{V}_i$ and V^0_i are the partial molar volume and molar volumes of either FeO or MgO. Data on the molar volume of the magnesiowüstite solid solution after equilibration at 1 bar and 1200 °C with metallic Fe are given by Nafziger and Muan (1967). These data, which consider all Fe as FeO, show a significant asymmetric deviation from Vergard's law. The Fe^{3+} and resultant non-stoichiometry of $Fe_{1-x}O$ have a significant effect on its molar volume, however, and the data need to be corrected for this in order to determine FeO–MgO excess volumes. The results of Srečec et al. (1987) show that $Fe^{3+}/(\Sigma Fe + Mg)$ goes below 0.005 for $Fe/(Fe + Mg) < 0.5$. At these concentrations Fe^{3+} will have a negligible effect on the lattice parameters. Therefore, if we discard the magnesiowüstite unit-cell data of Nafziger and Muan (1967) above $Fe/(Fe + Mg) = 0.5$ and use the estimated stochiometric FeO lattice parameter (Simons 1980), we find a smaller but still significant excess molar volume of mixing for the MgO–FeO solid solution which can be described by $W^{mw}_V = 0.0064$ J bar^{-1}.

Activity coefficients for the ringwoodite solid solution were then calculated from magnesiowüstite activities using the following expressions derived from integration of the Gibbs-Duhem equation (Wiser and Wood 1991).

$$\log \gamma^{ring}_{Fe} = -X^{ring}_{Mg} \log Q + \int_0^{X^{ring}_{Mg}} \log Q \, dX^{ring}_{Mg} \quad (18)$$

$$\log \gamma_{\mathrm{Mg}}^{\mathrm{ring}} = \log Q(1 - X_{\mathrm{Mg}}^{\mathrm{ring}}) + \int_{1}^{X_{\mathrm{Mg}}^{\mathrm{ring}}} \log Q \, \mathrm{d}X_{\mathrm{Mg}}^{\mathrm{ring}} \quad , \qquad (19)$$

where

$$\log Q = \log \left[\frac{a_{\mathrm{MgO}}^{\mathrm{mw}} X_{\mathrm{Fe}}^{\mathrm{ring}}}{a_{\mathrm{FeO}}^{\mathrm{mw}} X_{\mathrm{Mg}}^{\mathrm{ring}}} \right] \quad . \qquad (20)$$

The Fe concentrations of both oxide and silicate were corrected for the presence of Fe^{3+} as described previously. Using the above procedure with data from experiment no. 61 results in $W_{\mathrm{FeMg}}^{\mathrm{ring}}$ of 3.5 kJ mol^{-1} at 17.5 GPa and 1400 °C. A regular fit to the magnesiowüstite activities used gives $W_{\mathrm{FeMg}}^{\mathrm{mw}}$ of 12.3 kJ mol^{-1}. The partitioning data were then refitted with these values to give $\Delta G_{(1)}^{0}$ of 9.9 kJ mol^{-1}. Table 3 shows the results from following a similar procedure for data at pressures and temperatures where a sufficient range of Fe contents was measured. The refined values for $W_{\mathrm{FeMg}}^{\mathrm{ring}}$ vary little over this pressure and temperature range, while values for $W_{\mathrm{FeMg}}^{\mathrm{mw}}$ are changing by almost 2 kJ mol^{-1}. Values of $W_{\mathrm{FeMg}}^{\mathrm{mw}} - W_{\mathrm{FeMg}}^{\mathrm{ring}}$ are 8.5 ± 1 kJ mol^{-1}, which is in accordance with the value determined by least-squares fitting of Eq. (15).

The entire dataset at Fe saturation was then globally fitted using the data of Srečec et al. (1987) for the activity of magnesiowüstite and with the determined value of W_V^{mw}. Both $\Delta G_{(1)}^{0}$ and $W_{\mathrm{FeMg}}^{\mathrm{ring}}$ were initially allowed to vary linearly with pressure and temperature, but refined values of W_S^{ring} and W_V^{ring} were very small and were removed from the final refinement. That $W_V^{\mathrm{ring}} \approx 0$ is in accordance with the data of Akaogi et al. (1989) that show no excess volume of mixing for the ringwoodite solid solution. The fit resulted in a weighted χ squared of 1.11 with $|K_{D_{\mathrm{Obs}}} - K_{D_{\mathrm{Calc}}}|_{\mathrm{max}} = 0.5$ kJ. The fitted parameters are also given in Table 3 with $\Delta G_{(1)}^{0}$ expressed as $\Delta H - (T - 298)\Delta S + \Delta V(P)$. ΔS and ΔV are linear P and T dependencies of $\Delta G_{(1)}^{0}$ over the P and T range of the experiments. The global fit gives a value for $W_{\mathrm{FeMg}}^{\mathrm{ring}}$ of 3.5 ± 1 kJ mol^{-1}, which is about 200 J less than the average of the individually fitted values given in Table 3. Values of $\Delta G_{(1)}^{0}$ calculated from the global fit are also all within 200 J of the individually fitted values. Although a subregular model for the activity coefficient of magnesiowüstite was employed in the global fit, the equivalent symmetric interaction parameter ($W_{\mathrm{FeMg}}^{\mathrm{mw}}$) is equal to 12.1 ± 1.8 kJ mol^{-1} averaged over the experimental range of conditions.

Although we have insufficient data to combine Fe^{3+} measurements into a ternary thermodynamic model for this system, for experiments performed in Re capsules we can similarly correct the bulk Fe analyses for the presence of Fe^{3+} in order to examine the FeO–MgO partitioning at higher oxygen fugacity. If we assume a linear fit to the Fe^{3+} concentration in magnesiowüstite in Re capsules (Fig. 5b) and assume that the variation of Fe^{3+} in ringwoodite is the same as it is at Fe saturation, then the compositions of both phases can be corrected for Fe^{3+} content to estimate true FeO–MgO partitioning. This approach results in a $K_{D_{\mathrm{Fe}^{3+}}}^{\mathrm{ring/mw}}$ of approximately 0.1, which is lower than the range estimated for partitioning at Fe saturation. Figure 8 compares the raw Re data with those corrected for the Fe^{3+} content and shows the corrected data to be in quite good agreement with the best fit through the Fe-saturated data. We cannot, therefore, detect any influence on the Fe^{2+}–Mg^{2+} partitioning due to the presence of Fe^{3+}, and the main effect seems to be to increase the apparent bulk Fe content of magnesiowüstite.

Table 3 Interaction parameters for ringwoodite and magnesiowüstite

T (°C)	P (GPa)	$W_{\mathrm{Fe-Mg}}^{\mathrm{ring}}$ (kJ mol^{-1})	$W_{\mathrm{Fe-Mg}}^{\mathrm{mw}}$ (kJ mol^{-1})	$\Delta G°(1)$ (kJ mol^{-1})
1200	17.5	3.8(13)	11.3(10)	9.04(50)
1400	17.5	3.5(10)	12.3(7)	9.92(30)
1600	17.5	4.0(8)	12.7(8)	10.90(30)
1600	21.0	3.8(11)	13.0(10)	11.20(40)
Global fit		3.5(10)	12.1(18)	912 ± 150 + 4.15 ± 0.2 (T−298) + 18.9 ± 0.7(P); T in K, P in kbar

Comparison with previous studies

While the value for $W_{\mathrm{FeMg}}^{\mathrm{ring}}$ determined from the global fit to the Fe-saturated data is in good agreement with that of Matsuzaka et al. (2000), the values for $W_{\mathrm{FeMg}}^{\mathrm{mw}}$ and, therefore, $W_{\mathrm{FeMg}}^{\mathrm{mw}} - W_{\mathrm{FeMg}}^{\mathrm{ring}}$ are approximately 2 kJ higher in this previous work. This is almost certainly due to the presence of Fe^{3+}in the samples studied by Matsuzaka et al. (2000) that were also synthesised in Re capsules. Values of $\Delta G_{(1)}^{0}$ determined by Matsuzaka et al. (2000) are also 4.6 kJ higher than our measurements at 19 GPa and 1600 °C. The volume change predicted for Eq. (1) is

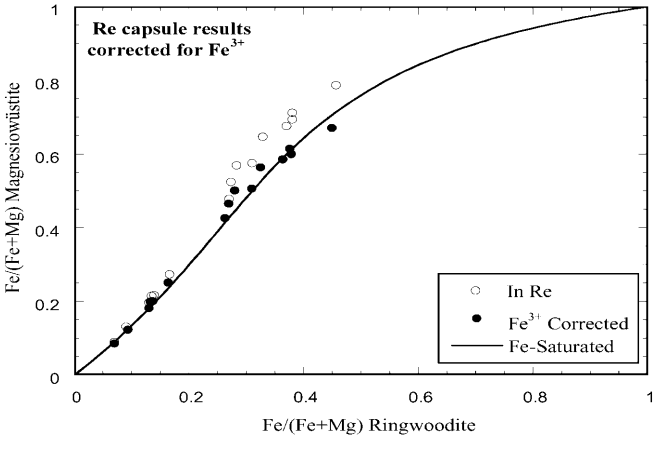

Fig. 8 Fe–Mg partitioning results from a Re capsule are shown with all Fe as FeO (*open circles*) and corrected for the presence of Fe^{3+} in both phases using EELS data (*filled circles*). There is good agreement between the corrected data and the results from experiments performed at metallic Fe saturation

much smaller than that calculated from the equation of state data used by Matsuzaka et al. (2000). Other compilations of equation of state data also overestimate this volume change (Fei et al. 1991; Chatterjee et al. 1998). At 17.5 GPa and 1600 °C the data used by Matsuzaka et al. (2000), for example, predict a volume change of 0.8 cm^3 mol^{-1}. Our refined value of 0.19 cm^3 mol^{-1} is much closer to the room pressure and temperature volume change of 0.27 cm^3 mol^{-1}, which might mean that the equation of state parameters for the four phases are in reality much more similar or tend to cancel out on each side of Eq. (1). It is clear from the lack of variation in the partitioning data over quite a large pressure range that $\Delta V_{(1)}$ must be quite small. The partitioning results are therefore quite a sensitive and independent test of equation of state data, and it is apparent that some of the equation of state parameters available in the literature and used in phase equilibria calculations are inconsistent with our results. This is perhaps not surprising, as very few equation of state measurements have been made at simultaneous high pressure and temperature, and almost no data exist up to temperatures of 1600 °C at high pressure. It is difficult to determine exactly which values may be in error, but values can be found from the range available in the literature to bring the calculated volume change of Matsuzaka et al. (2000) into accordance with our determination. The unit-cell volume for end member Fe-ringwoodite can be reduced to 41.86 cm^3 mol^{-1} (O'Neill et al. 1993). A lower value of -0.04 GPa K^{-1} (Plymate and Stout 1994) can be used for $(\partial K_T/\partial T)_P$ of Fe_2SiO_4 ringwoodite. The bulk modulus of stoichiometric end-member FeO can be increased to 180 GPa in accordance with the findings of Zhang (2000). When these data are used with the remaining data and equations given by Matsuzaka et al. (2000), the volume change of Eq. (1) is brought into accordance with that determined in our study. On the other hand, due to the uncertainties in current equation of state data and the absence of simultaneous high P and T measurements, using the volume change at room P and T for such ion-exchange reactions may result in a more reliable estimate.

Using the thermodynamic data determined in this study and data consistent with this study, we can calculate the breakdown reaction of ringwoodite to magnesiowüstite plus stishovite for a system without Fe^{3+}. The method followed is the same as that described by Matsuzaka et al. (2000). The two equilibria for the end-member components in this reaction are:

$$\begin{matrix} Mg_2SiO_4 & = & 2MgO & + & SiO_2 \\ \text{ring} & & \text{mw} & & \text{stish} \end{matrix} \tag{21}$$

$$\begin{matrix} Fe_2SiO_4 & = & 2FeO & + & SiO_2 \\ \text{ring} & & \text{mw} & & \text{stish} \end{matrix} . \tag{22}$$

The free energy changes for Eqs. (21) and (22), which are both equal to zero at equilibrium, are then given as:

$$\Delta H_{(21)1\text{bar},T} + T\Delta S_{(21)1\text{bar},T} + \int_{1\text{bar}}^{P} \Delta V_{(21)T}\,\mathrm{d}P + RT\ln\left(\left[a_{\text{MgO}}^{\text{mw}}\right]^2 \Big/ \left[a_{\text{Mg}_2\text{SiO}_4}^{\text{ring}}\right]\right) = 0 \tag{23}$$

$$\Delta H_{(22)1\text{bar},T} + T\Delta S_{(22)1\text{bar},T} + \int_{1\text{bar}}^{P} \Delta V_{(22)T}\,\mathrm{d}P + RT\ln\left(\left[a_{\text{FeO}}^{\text{mw}}\right]^2 \Big/ \left[a_{\text{Fe}_2\text{SiO}_4}^{\text{ring}}\right]\right) = 0 \tag{24}$$

Using thermodynamic data and the equations for heat capacity and thermal expansion given by Matsuzaka et al. (2000), Eqs. (23) and (24) were solved simultaneously to give the coexisting compositions of ringwoodite and magnesiowüstite. Thermodynamic parameters were adjusted in the following way, however, to fit the partitioning data collected at metallic Fe saturation in our study. Firstly, the equations of state data were changed as previously outlined to fit our smaller value for $\Delta V_{(1)}$. Then ΔH^0_{298} and ΔS^0_{298} for Fe_2SiO_4 ringwoodite were changed such that the calculated conditions for the end-member equilibrium (Eq. 22) were in agreement with the phase equilibria determinations of Katsura et al. (1998) for this reaction at metallic Fe saturation. Finally, ΔH^0_{298} and ΔS^0_{298} for Mg_2SiO_4 ringwoodite were adjusted to bring $\Delta G^0_{(1)}$ into agreement with our determined value. The augmented thermodynamic data are given in Table 4. Values for $W^{\text{mw}}_{\text{FeMg}}$ and $W^{\text{ring}}_{\text{FeMg}}$ were taken from our global fit to the partitioning data.

Figure 9 shows the results of this calculation compared with the experimental and calculated phase boundaries of Matsuzaka et al. (2000) and the phase equilibria data of Ito and Takahashi (1989). There is good agreement between all three studies for the equilibrium composition of ringwoodite, although in the study of Ito and Takahashi (1989) the Fe content of ringwoodite at the breakdown to perovskite and magnesiowüstite is around 5% lower. There is, however, a marked divergence in the coexisting magnesiowüstite composition between our study and that of Matsuzaka et al. (2000). As previously discussed, this is most likely due to the use of Re capsules by Matsuzaka et al. and to the consequent higher Fe^{3+} concentration of magnesiowüstite. In addition, the larger predicted $\Delta V_{(1)}$ in this previous study results in an increase in the apparent Fe content of magnesiowüstite with pressure and divergence between the two studies.

Reducing the Fe^{3+} content of the experiments and establishing oxidation conditions more applicable to the Earth's transition zone therefore results in an apparent narrowing of the pressure interval over which ringwoodite, of a particular Fe content, would break down to oxides. For example, ringwoodite with $Fe/(Fe+Mg) = 0.7$ will break down over a pressure interval which is approximately 30% smaller if results from Fe capsules

Table 4 Thermodynamic data used in the calculation shown in Fig. 9

	V_{298} (cm^3 mol^{-1})	ΔH°_{298} (kJ mol^{-1})	ΔS°_{298} (J/mol K^{-1})	K_T (GPa)	K'_T	$\left(\frac{\partial K_T}{\partial T}\right)_P$ (GPa K^{-1})
Mg_2SiO_4 ring	39.487	−2137.9[c]	84.6[c]	182.6	5	−0.0284
Fe_2SiO_4 ring[a]	41.860[b]	−1471.5[c]	141.0[d]	192.0	5	−0.04[f]
MgO mw	11.248	−601.5[d]	26.9[d]	160.3	4.1	−0.034[h]
FeO mw	12.250	−267.3[d]	57.59[d]	180.0[g]	4[g]	−0.027
SiO_2 stish	14.014	−873.7[e]	27.2[e]	314.0	5.1	−0.047

[a] All data from Matsuzaka et al. (2000) except [b] O'Neill et al. (1993), [c] this study, [d] Fei et al. (1991), [e] Akaogi et al. (1995), [f] Plymate and Stout (1994), [g] Zhang (2000), [h] Utsumi et al. (1998)

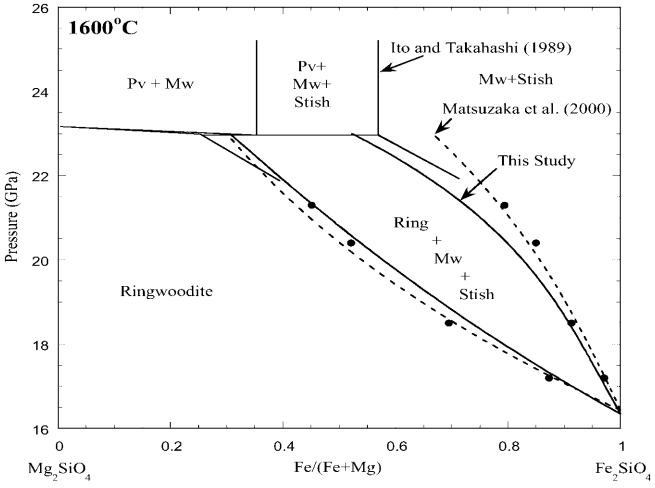

Fig. 9 Phase diagram at 1600 °C for the breakdown of ringwoodite to magnesiowüstite plus stishovite calculated from the partitioning experiments performed at metallic Fe saturation. The phase equilibria data of Matsuzaka et al. (2000) performed in Re capsules are shown (*filled circles*) with their calculated equilibrium curves (*broken lines*). The transition boundaries determined by Ito and Takahashi (1989) are shown in *grey*. *Pv* refers to (Mg,Fe)SiO_3 perovskite; *Mw* is magnesiowüstite; *Stish* is stishovite

are used, in comparison to the results under more oxidising conditions. Although the reaction involving ringwoodite studied here is not directly applicable to the Earth's interior, the results highlight how the pressure interval of an Fe-bearing phase transformation may be broadened at high oxygen fugacity if Fe^{3+} partitions more strongly into one of the phases.

The major uncertainties in our calculation arise from the determination of the pressure and the use of other thermodynamic data. As the pressure in the multianvil assembly was calibrated using Eq. (22) in the presence of metallic Fe, the calculation should be at least internally consistent even if the absolute pressure of the end-member reaction is incorrect. Furthermore, as the pressure effect on the partitioning data is small, large uncertainties in the pressure have little effect on the determined thermodynamic properties. One concern is in the extrapolation of the Srečec et al. (1987) data for the activity composition relations of magnesiowüstite to 1600 °C, which is over 400 °C above their measured range. These data predict an increase in $W^{\mathrm{mw}}_{\mathrm{FeMg}}$ with temperature; however, in reality this value may start to decrease at some temperature. The calculation in Fig. 9, however, is more dependent on the value of $W^{\mathrm{mw}}_{\mathrm{FeMg}} - W^{\mathrm{ring}}_{\mathrm{FeMg}}$, which is very well constrained by our partitioning data, than the value for $W^{\mathrm{mw}}_{\mathrm{FeMg}}$ used. If $W^{\mathrm{mw}}_{\mathrm{FeMg}}$ is changed by ±3 kJ while keeping $(W^{\mathrm{mw}}_{\mathrm{FeMg}} - W^{\mathrm{ring}}_{\mathrm{FeMg}})$ constant, the effect on the coexisting compositions in Fig. 9 at 21 GPa is less than 1.5 mol%. The changes made to the equation of state data, although based on observations in the literature, are not necessarily the correct values, they are simply consistent with our measurement of $\Delta V_{(1)}$. We can change different sets of equation of state data but, with the exception of those for stishovite, as long as the calculated value for $\Delta V_{(1)}$matches our measured value, the calculated boundaries in Fig. 9 will remain unchanged.

Finally, an interesting observation is that in Fe capsules the assemblage ringwoodite, magnesiowüstite and stishovite was never observed. Although some starting compositions had very high initial Fe contents, the maximum Fe content of ringwoodite and magnesiowüstite was always less than the compositions in equilibrium with stishovite calculated in Fig. 9. In Re capsules, on the other hand, assemblages of these three phases were observed and the maximum Fe contents for ringwoodite were close to those shown in Fig. 9. This can be explained by differences in the redox buffering reactions that come into operation in the presence or absence of stishovite. When ringwoodite and magnesiowüstite coexist with metallic Fe the oxygen fugacity is buffered by Eq. (2). When ringwoodite starts to break down to stishovite, however, the oxygen fugacity is described by the reaction:

$$\underset{\text{metal}}{2\mathrm{Fe}} + \underset{\text{stish}}{\mathrm{SiO_2}} + \mathrm{O_2} = \underset{\text{ring}}{\mathrm{Fe_2SiO_4}} \quad . \tag{25}$$

If the oxygen fugacity of Eq. (25) is below that of Eq. (2), as thermodynamic data suggest, then Fe in magnesiowüstite will be reduced to metal with the appearance of stishovite. It is therefore not possible for ringwoodite, magnesowüstite and stishovite to coexist in the presence of metallic Fe. What seems to occur in the experiments is that subsequent partitioning then shifts the compositions of both magnesiowüstite and ringwoodite to lower Fe contents. In this way, the Fe contents of the silicate and oxide phases are buffered at values below the breakdown of the silicate phase. There

may be implications from this observation for the oxygen fugacity and FeO content at the top of the lower mantle during core formation.

Summary

Activity–composition relations for the ringwoodite solid solution have been evaluated from Fe–Mg partitioning data between ringwoodite and magnesiowüstite performed in the presence of metallic Fe. The determined value for $W^{mw}_{FeMg} - W^{ring}_{FeMg}$ is 8.5 ± 1 kJ mol^{-1}.

A global fit to the partitioning data between 17 and 23 GPa and 1200 and 1600 °C gives $W^{ring}_{FeMg} = 3.5 \pm 1$ kJ mol^{-1} using an existing activity composition model for magnesiowüstite. No pressure or temperature variation was discernible for W^{ring}_{FeMg}, the value of which is in good agreement with that determined by Matsuzaka et al. (2000). Although the activity model used for magnesiowüstite includes P and T variables, the equivalent regular interaction parameter (W^{mw}_{FeMg}) is 12.1±1.8 kJ mol^{-1} over the experimental conditions.

The free energy change in J mol^{-1} for the exchange reaction (Eq. 1) can be described by $912 + 4.15\,(T - 298) + 18.9\,P$ with T in K, P in kbars. The volume change for this reaction is smaller than predicted by current compilations of internally consistent equation of state data, but is close to the room P and T volume change. Due to the uncertainties in currently available equation of state data, room P and T estimates for the ΔV of an ion exchange reaction may be more reliable.

Differences in apparent Fe–Mg partitioning are observed between experiments performed in Fe and Re capsules, due to higher Fe^{3+} concentrations in the latter experiments. EELS data show that Fe^{3+} partitions preferentially into magnesiowüstite over ringwoodite. The Fe^{3+} distribution coefficient ($K^{ring/mw}_{D_{Fe^{3+}}}$) in the presence of metallic Fe is estimated to be between 0.3 and 0.6 over the range of experimental compositions. Magnesiowüstite Fe^{3+} concentrations are approximately three times higher for samples produced in Re capsules than in Fe capsules.

The polysynthetic twins parallel to (3 1 1) observed in magnetite formed at 21 GPa and 1600 °C and the low Fe^{3+} content of coexisting magnesiowüstite may be evidence that magnetite existed in a high-pressure form but went through a subsequent retrograde transformation during decompression.

The presence of Fe^{3+} in phases produced in multianvil experiments using Re capsules can have a marked effect on the apparent phase relations and determined thermodynamic properties. Experiments performed on Fe-bearing systems in equilibrium with metallic Fe are likely to be more applicable to the oxidation state of the Earth's transition zone and lower mantle.

Acknowledgements We are grateful for discussions with C. McCammon, R. Angel, T. Gasparik, H. O'Neill and B. Wood. We also thank G. Herrmannsdörfer, H. Fischer, H. Schultz and D. Krauße for their technical assistance. High-pressure multianvil experiments at the Bayerisches Geoinstitut are supported by the EU TMR-Large Scale Facilities programme (Contract no. ERB-FMGECT980111 to D.C. Rubie).

References

Akaogi M, Ito E, Navrotsky A (1989) Olivine-modified spinel–spinel transitions in the system Mg_2SiO_4-Fe_2SiO_4: calorimetric measurements, thermochemical calculation, and geophysical application. J Geophys Res 94: 15671–15685

Akaogi M, Yusa H, Shiraishi K, Suzuki T (1995) Thermodynamic properties of α-quartz, coesite and stishovite and equilibrium phase relations at high pressures and high temperatures. J Geophys Res 100: 22337–22347

Akaogi M, Kojitani H, Matsuzaka K, Suzuki T, Ito E (1998) Post-spinel transformations in the system Mg_2SiO_4-Fe_2SiO_4: element partitioning, calorimetry and thermodynamic calculation. In: Manghnani MH, Yagi T (eds) High pressure-temperature research: properties of Earth and planetary materials. Am Geophys Union, Washington, DC, pp 373–384

Benz HM, Vidale JE (1993) Sharpness of upper-mantle discontinuities determined from high-frequency reflections. Nature 365: 147–150

Binns RA, Davis RJ, Reed SJB (1969) Ringwoodite, natural (Mg, Fe)$_2SiO_4$ spinel in the Tenham meteorite. Nature 221: 943–944

Canil D, O'Neill HStC, Ross II CR (1991) A preliminary look at phase relations in the system γ-Fe_2SiO_4–Fe_3O_4 at 7 GPa. Terra Abstr 3: 65

Chatterjee ND, Kruger R, Haller G, Olbricht W (1998) The Bayesian approach to an internally consistent thermodynamic database: theory, database, and generation of phase diagrams. Contrib Mineral Petrol 133: 149–168

Chopelas A, Boehler R, Ko T (1994) Thermodynamics and behavior of γ-Mg_2SiO_4 at high pressure: implications for Mg_2SiO_4 phase equilibrium. Phys Chem Miner 21: 351–359

Fei Y, Saxena SK, Navrotsky A (1990) Internally consistent thermodynamic data and equilibrium phase relations for compounds in the system MgO–SiO_2 at high pressure and high temperature. J Geophys Res 95: 6915–6928

Fei Y, Mao HK, Mysen BO (1991) Experimental element partitioning and calculation of phase relations in the MgO–FeO–SiO_2 system at high pressure and high temperature. J Geophys Res 96: 2157–2169

Fei Y, Frost DJ, Mao HK, Prewitt C, Häusermann D (1999) In situ structure determination of the high-pressure phase of Fe_3O_4. Am Mineral 84: 203–206

Fisher GW, Medaris LG (1969) Cell dimensions and X-ray determinative curve for synthetic Mg–Fe olivines. Am Mineral 54: 741–753

Haavik CH, Stølen S, Fjellvåg H, Hanfland M, Häusermann D (2000) Equation of state of magnetite and its high-pressure modification: thermodynamics of the Fe–O system at high pressure. Am Mineral 85: 514–523

Irifune T, Nishiyama N, Kuroda K, Inoue T, Isshiki M, Utsumi W, Funakoshi K, Urakawa S, Uchida T, Katsura T, Ohtaka O (1998) The postspinel phase boundary in Mg_2SiO_4 determined by in situ X-ray diffraction. Science 279: 1698–1700

Ito E, Takahashi E (1989) Postspinel transformations in the system Mg_2SiO_4–Fe_2SiO_4 and some geophysical implications. J Geophys Res 94: 10637–10646

Katsura T, Ito E (1989) The system Mg_2SiO_4–Fe_2SiO_4 at high pressures and temperatures: precise determination of stabilities of olivine, modified spinel and spinel. J Geophys Res 94: 15663–15670

Katsura T, Ueda A, Ito E, Morooka K (1998) Postspinel transition in Fe_2SiO_4. In: Manghnani MH, Yagi T (eds) High pressure-temperature research: properties of Earth and planetary materials. Am Geophys Union, Washington DC, pp 435–440

McCammon C (1993) Effect of pressure on the composition of the lower-mantle end-member Fe_xO. Science 259: 66–68

McCammon C, Peyronneau J, Poirier JP (1998) Low ferric iron content of (Mg,Fe)O at high pressures and temperatures. Geophys Res Lett 25: 1589–1592

Matsuzaka K, Akaogi M, Suzuki T, Suda T (2000) Mg–Fe partitioning between silicate spinel and magnesiowüstite at high pressures: experimental determination and calculation of phase relations in the system Mg_2SiO_4–Fe_2SiO_4. Phys Chem Miner 27: 310–319

Morishima H, Kato T, Suto M, Ohtani E, Urakawa S, Utsumi W, Shimomura O, Kikegawa T (1994) The phase boundary between α- and β-Mg_2SiO_4 determined by in situ X-ray observation. Science 265: 1202–1203

Nafziger RH, Muan A (1967) Equilibrium phase compositions and thermodynamic properties of olivines and pyroxenes in the system MgO–"FeO"–SiO_2. Am Mineral 52: 1365–1385

O'Neill HstC (1988) Systems Fe–O and Cu–O: thermodynamic data for the equilibria Fe–"FeO", Fe–Fe_3O_4, "FeO"–Fe_3O_4, Fe_3O_4–Fe_2O_3, Cu–Cu_2O and Cu_2O–CuO from EMF measurements. Am Mineral 73: 470–486

O'Neill HstC, Rubie DC, Canil D, Geiger CA, Ross CR, Seifert F, Woodland AB (1993) Ferric iron in the upper mantle and in transition zone assemblages: implications for relative oxygen fugacities in the mantle. Geophys Monograph 74 IUGG vol 14 73–89

Plymate TG, Stout JH (1994) Pressure-volume-temperature behaviour of γ-Fe_2SiO_4 (spinel) based on static compression measurements at 400 °C. Phys Chem Miner 21: 413–420

Pownceby MI, O'Neill HstC (1994) Thermodynamic data from redox reactions at high temperature. IV. Calibration of the Re–ReO_2 oxygen buffer from EMF and NiO + Ni–Pd redox sensor measurements. Contrib Mineral Petrol 118: 130–137

Simons B (1980) Composition–lattice parameter relationship of the magnesiowüstite solid solution series. Carnegie Inst Washington Yb 79: 376–380

Speidel DH (1967) Phase equilibria in the system MgO–FeO–Fe_2O_3. The 1300 °C isothermal section and extrapolations to other temperatures. Am Ceram Soc J 50: 243–247

Srečec I, Ender A, Woermann E, Gans W, Jacobsson E, Eriksson G, Rosén E (1987) Activity–composition relations of the magnesiowüstite solid solution series in equilibrium with metallic iron in the temperature range 1050–1400 K. Phys Chem Miner 14: 492–498

Suzuki A, Ohtani E, Morishima H, Kubo T, Kanbe Y, Kondo T (2000) In situ determination of the phase boundary between wadsleyite and ringwoodite in Mg_2SiO_4. Geophys Res Lett 27: 803–806

Utsumi W, Weidner DJ, Liebermann RC (1998) Volume measurement of MgO at high pressure and temperature. In: Maghnani MH, Yagi T (eds) Properties of Earth and planetary materials at high pressure and temperature. Am Geophys Union, Washington, DC, pp 327–334

van Aken PA, Liebscher B, Styrsa VS (1998) Quantitative determination of iron oxidation states in minerals using Fe L2,3-edge electron energy-loss near-edge structure spectroscopy. Phys Chem Miner 5: 323–327

van Cappellen E, Doukhan JC (1994) Quantitative X-ray microanalysis of ionic compounds. Ultramicroscopy 53: 343–349

Walker D, Carpenter MA, Hitch CM (1990) Some simplifications to multianvil devices for high-pressure experiments. Am Mineral 75: 1020–1028

Wiser N, Wood BJ (1991) Experimental determination of activities in Fe–Mg olivine at 1400 K. Contrib Mineral Petrol 108: 146–153

Wood BJ, Rubie DC (1996) The effect of alumina on phase transformations at the 660-kilometer discontinuity from Fe–Mg partitioning experiments. Science 273: 1522–1524

Woodland AB, Angel RJ (2000) Phase relations in the system fayalite–magnetite at high pressures and temperatures. Contrib Mineral Petrol 139: 734–747

Yagi T, Akaogi M, Shimomura O, Suzuki T, Akimoto S (1987) In situ observation of the olivine–spinel phase transition in Fe_2SiO_4 using synchrotron radiation. J Geophys Res 92: 6207–6213

Zhang J (2000) Effect of defects on the elastic properties of wüstite. Phys Rev Lett 84: 507–510